Eur. Phys. J. D (2013) 67: 230
DOI: 10.1140/epjd/e2013-40422-9

THE EUROPEAN PHYSICAL JOURNAL D

Regular Article

Resonant electron attachment to polar aromatic molecules: consequences for their chemistry in the interstellar medium*

Fabio Carelli[1], Mauro Satta[2] and Franco A. Gianturco[1,a]

[1] Department of Chemistry and CISM, The University of Rome 'Sapienza', P.le Aldo Moro 5, 00185 Rome, Italy
[2] CNR-ISMN, P.le Aldo Moro 5, 00185 Rome, Italy

Received 16 July 2013 / Received in final form 31 August 2013
Published online 15 November 2013 –

Abstract. In this paper we present and discuss the results obtained from ab-initio quantum scattering calculations of the response from neutral aromatic species like C_6H_5 (phenyl) and C_6H_4 (benzyne, ortho isomer) to low-energy electron collisions. Our main purpose is to investigate the possible mechanisms that can lead to the final formation of their stable negative ions under astrophysical conditions, by linking low-lying metastable anionic states to bound anionic states. Quantum chemical calculations were also employed to confirm the features of the metastable resonant states found by the scattering calculations, while the role of the permanent dipole moments of both systems on the scattering behaviour for near-threshold electrons is also analysed in some detail. The possible energy redistribution paths for stabilizing both anionic species under ISM conditions are discussed in the conclusions.

1 Introduction

Polycyclic aromatic hydrocarbons (PAHs) have been considered for a long time to be abundant and ubiquitous in the interstellar medium (ISM) [1–5], even though currently no specific chemical carrier has been unambiguously identified [6,7] with the exception of benzene (C_6H_6, [8]). These molecules are also taken as prebiotic species (as important carbon-bearing species, [9]) and are surmised to store ∼5% of the elemental carbon, a carbon reservoir which is comparable to that of gaseous CO [10].

In connection with the molecular synthesis which are taken to occurr in the stellar wind of C-rich AGB stars, at present it is well known that the carbon element, synthesized through helium burning reactions in the core of the star, is then dredged up to the photosphere due to convective transport mechanisms so that it reacts there with the elemental oxygen-forming CO.

Since AGB stars undergo extensive mass losses at high rates, (up to 10^{-4} $M_\odot$ yr^{-1}, [11,12], $M_\odot = 1.9884 \times 10^{+30}$ kg being the solar mass), the circumstellar material is physically processed due to an intense stellar wind; accordingly, free gas-phase PAHs are thought to form either in the ejecta from C-rich post-AGB stars or in evolved proto-planetary nebulae (PPN) objects as critical intermediaries and by-products of the dust formation processes. It therefore follows that the spectroscopic detection of organic aromatic compounds, both in the circumstellar environments (CSE) and in the ejecta of C-rich evolved stars, indirectly provide precious information on how these species are formed: hence, the fact that no aromatic infrared bands (AIBs) have been seen in AGB stars, the AIBs making instead their appearence either in the post-AGB or PPN objects, strongly suggests that the aromatic species might be synthesized mainly during the post-AGB phase of C-rich stars [13–15].

In this framework, it is interesting that in almost all of the above mechanisms the phenyl-radical is being considered as one of the chemical cornerstones toward the production of larger carbonaceous polycyclic species. In this sense, C_6H_5 clearly represents one of the building blocks for PAHs formation so that its chemistry and more in general that of benzene-related species, like the aromatic single-ring containing orthobenzyne, o-C_6H_4, and the phenyl radical C_6H_5 that we shall analyse in the present work, are considered prototypical toward the formation of larger aromatic species in the above astrophysical environments. It is additionally thought that low-energy collisions with free electrons, whose presence may be found either in the stellar wind or in the local photoionization of interstellar/circumstellar matter (including dense molecular clouds), can participate to the above complex synthetic mechanisms by forming either low-energy 'compound' resonances or virtual states by which it is in turn possible to access a variety of stable negative ions via several energy-redistribution paths. In our earlier work [16,17] another likely PAH precursor, the closed shell neutral orthobenzyne was found to exhibit strong

* Contribution to the Topical Issue "Electron and Positron Induced Processes", edited by Michael Brunger, Radu Campeanu, Masamitsu Hoshino, Oddur Ingólfsson, Paulo Limão-Vieira, Nigel Mason, Yasuyuki Nagashima and Hajime Tanuma.

[a] e-mail: francesco.gianturco@uniromal.it

interactions with low-energy electrons. Those findings enabled us to suggest direct involvement of its associated anion within the complex chain of reactions leading to the formation of the larger PAHs, hence we find it reasonable that another aromatic (open-shell) system should be involved both in the ISM and in protoplanetary atmospheres: the phenyl radical. It has a comparatively larger electron affinity (EA_{phenyl} = 1.0960 ± 0.0060 eV [18], while $EA_{o-benzyne}$ = 0.5640 ± 0.0070 eV [19]) but a lower dipole moment: μ_{phenyl} = 0.872 D/0.9 D, the former computed at the ROB3LYP/aug-cc-pVTZ expansion level by us, the latter experimentally determined by [20]. For the o-C_6H_4 case, $\mu_{o-benzyne}$ = 1.68 D/1.77 D, the former referring to the theoretical value [21] and the latter having been computationally evaluated by us [16] at the B3LYP/aug-cc-pVTZ level.

PAHs species in the ISM have been tentatively included in some astrochemical models [22,23] where their inclusion is shown to have remarkable consequences. In this framework, the phenyde anion ($C_6H_5^-$) constitutes a very likely archetype since the neutral (not deprotonated) counterpart is the benzene molecule which has instead a large negative EA. Since the astrochemical models that currently include PAHs do not yet account for the dehydrogenated anionic polycyclic aromatic species (generally identified as PAH^-_{n-1}), it therefore follows that it is important to start to characterize the kinetics of formation of this class of anions: accordingly, we focus here on the mechanisms that, at the nanoscopic level, can yield the phenyde metastable anionic species as the doorway for the formation of the thermodynamically stable phenyde anion, whose gas-phase reactivity with species of interstellar relevance has been recently experimentally probed [24] with very similar conclusions.

The main purpose of the present work is therefore to assess the existence of low-energy resonances as doorways to the formation of the associated stable negative ions under the astrophysical conditions typical either of dense molecular clouds or of circumstellar environments; moreover, due to the permanent dipole moments of both molecules, we shall investigate the occurrence of very low-energy dipole quasi-bound state as another likely option that can help to stabilize bound anions of both the C_6H_5 and C_6H_4 molecular partners via different, possible energy redistribution paths after the initial electron attachment into a resonant state.

2 An outline of the scattering calculations

Since the quantum dynamical equations used for this study have been described in detail many times before [25,26], we only present here a brief outline of it and refer the reader interested in more details to those earlier publications.

The total $(N+1)$-electron wave function is constructed as an antisymmmetrized product of one-electron wave functions obtained from Hartree-Fock orbitals of the neutral ground state molecular target, considering the N bound electrons in their ground-state configuration during the whole scattering process: thus, no core-excited resonances are allowed in our modelling. Each of the three dimensional wave functions describing a given electron is expanded around the molecular center of mass (Single Center Expansion, SCE, [25]) so that for each of the bound molecular electrons we have

$$\phi_i^{p\mu} = \frac{1}{r}\sum_{\ell h} u_{\ell h}^{p\mu,i}(r)\chi_{\ell h}^{p\mu}(\hat{r};\mathbf{R}) \tag{1}$$

and for the scattered particle

$$\psi^{p\mu} = \frac{1}{r}\sum_{\ell h} f_{\ell h}^{p\mu}(r)\chi_{\ell h}^{p\mu}(\hat{r};\mathbf{R}). \tag{2}$$

In the above SCE representations, the superscripts label the μth irreducible representation of the pth symmetry group to which the molecule belongs at the fixed nuclear geometry $\mathbf{R}$, and the subscripts refer to each of the angular channels under consideration; the radial coefficients $u_{\ell h}^{p\mu,\alpha}$ for the bound molecular electrons are numerically evaluated by a quadrature on a radial grid [27]. The angular functions $\chi_{\ell h}^{p\mu}$ are given as:

$$\chi_{\ell h}^{p\mu} = \sum_m b_{\ell h m}^{p\mu} Y_\ell^m(\hat{r}), \tag{3}$$

where the $b_{\ell h m}^{p\mu}$ coefficients are described and tabulated in reference [28]. The ensuing coupled partial integro-differential quantum scattering equations evaluate the unknown radial coefficients $f_{\ell h}^{p\mu}$ for the $(N+1)$th continuum electron:

$$\left[\frac{d^2}{dr^2} - \frac{l(l+1)}{r^2} + 2\left(E-\epsilon\right)\right] f_{lh}^{p\mu}(r|\mathbf{R}) = 2\sum_{l'h'}\int dr' \hat{V}_{lh,l'h'}^{p\mu}(r,r'|\mathbf{R}) f_{l'h'}^{p\mu}(r'|\mathbf{R}), \tag{4}$$

where E is the collision energy and ϵ is the eigenvalue for the electronic ground state energy so that $k^2/2 = E-\epsilon$, k being the asymptotic momentum of the elastically scattered electron.

For a target which has a closed shell electronic structure, with $n_{occ} = N/2$ doubly occupied molecular orbitals, the static-exchange (SE) potential has the following form:

$$V_{SE}(\mathbf{r}) = \sum_{\gamma=1}^{M}\frac{Z_\gamma}{|\mathbf{r}-\mathbf{R}_\gamma|} + \sum_{i=1}^{n_{occ}}\left(2\hat{J}_i - \hat{K}_i\right) = V_{st} - \sum_{i=1}^{n_{occ}}\hat{K}_i \tag{5}$$

where $\hat{J}_i$ and $\hat{K}_i$ are the usual local static potential and the non-local exchange potential operators respectively. We further model the correlation and polarization effects via the following optical potential:

$$V_{cp}(r) = \begin{cases} V_{corr}(r) & r \le r_{match} \\ V_{pol}(r) & r > r_{match}. \end{cases} \tag{6}$$

We then generate the exchange interaction with the Free-Electron-Gas-Exchange model proposed by Hara (HFEGE, [29]), V_{HFEGE}

$$V_{HFEGE}(\mathbf{r}|\mathbf{R}) = -\frac{2}{\pi}K_F(\mathbf{r}|\mathbf{R})\left[\frac{1}{2}+\frac{1-\eta^2}{4\eta}\ln\left(\frac{1+\eta}{1-\eta}\right)\right]. \tag{7}$$

When dealing with an *open*-shell system as in the case of C_6H_5, the electronic density $\rho(\mathbf{r}|\mathbf{R})$

$$\rho(\mathbf{r}) = \int |\det||\phi_1(\mathbf{r})\phi_2(\mathbf{x}_2)\cdots\phi_{n_e}(\mathbf{x}_{n_e})||^2 d\mathbf{x}_2 d\mathbf{x}_3\cdots d\mathbf{x}_{n_e} \tag{8}$$

is evaluated by assigning 2 as the occupation number of each of the 20 doubly occupied MO in the neutral target and by setting such value equal to 1 for the X^2A_1 radical electron: in this way we treat 'exactly' (in the limit of the HFEGE model for the exchange contribution) the exchange interaction between the colliding electron and each of the 'core' doubly occupied MOs, while keeping for the uncoupled bound electron an 'hybrid' description which is in between a triplet/singlet coupling with the impinging electron, as done in our earlier work [30]. We therefore expect the present cross sections to be located in size between the correct singlet and triplet cross sections for the phenyl radical.

This last step provides the so-called static-model-exchange-correlation-polarization (SMECP) potential accounting for the interaction forces between the impinging free electron and the target molecule. The coupled set of integrodifferential equations now takes the form

$$\left[\frac{d^2}{dr^2}-\frac{l(l+1)}{r^2}+k^2\right] f_{lh}^{p\mu}(r) = 2\sum_{l'h'} V_{lh,l'h'}^{p\mu}(r) f_{l'h'}^{p\mu}(r), \tag{9}$$

where the potential coupling elements are

$$\begin{aligned} V_{lh,l'h'}^{p\mu}(r) &= \langle \chi_{lh}^{p\mu}(\hat{r})|V(\mathbf{r})|\chi_{l'h'}^{p\mu}(\hat{r})\rangle \\ &= \int d\hat{r}\chi_{lh}^{p\mu}(\hat{r})V(\mathbf{r})\chi_{l'h'}^{p\mu}(\hat{r}). \end{aligned} \tag{10}$$

The numerical solutions of the coupled equations produce the relevant K-matrix elements which will in turn yield the final integral cross sections [31].

3 Results and discussion

3.1 Numerical details: the phenyl target

The computed and experimental values of the permanent dipole moment and of dipole polarizabilities, have been presented and discussed for the closed-shell benzyne molecule in our earlier work of [16]. We shall therefore not repeat those data in the present manuscript, while discussing with more details the calculations which refer to the C_6H_5 system.

The molecular orbitals of the equilibrium structure of the C_6H_5 molecule were obtained at the ROHF level by using the aug-cc-pVTZ basis set [32]. The molecular structure obtained by geometry optimization with the same basis set is reported in Figure 1.

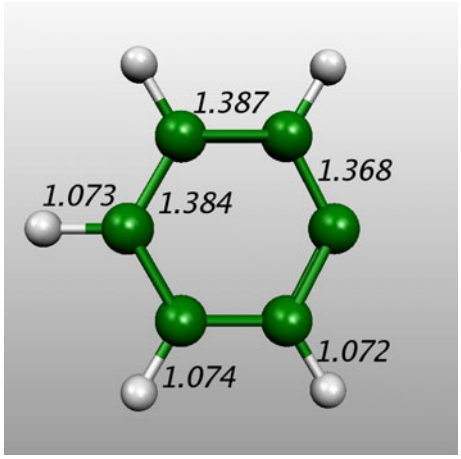

Fig. 1. Optimized equilibrium nuclear structure for the phenyl radical; the bond distances are in Angstrom. See text for details.

The present calculations yield a permanent dipole moment of 0.872 D, and a tensorial polarizability whose components are 44.05, 82.02 and 77.68 Bohr^3 (xx, yy and zz, respectively).

The largest contributing angular momentum value for the scattered electron which we have included in the calculations was LMax = 60, so that the interaction potential was expanded using lmax = 120 partial waves. The size of the physical box containing the above potential terms to describe the electron-molecule collision was finally fixed at 50 Å. To ensure that the final cross sections are numerically converged all the necessary indicators of numerical convergence were consequently tested: no substantial variation of our results occurs with the increasing both the box size and the number of partial waves included in equation (10).

3.2 The low-energy resonances of phenyl radical

The low-energy behaviour of our elastic, rotationally summed, computed ICS are reported in Figure 2 for the two contributing partial cross sections for which resonant features have been found. The data, in fact, indicate the presence of a broad maximum arising from the coalescence of two well resolved resonances. Both of them are confirmed by the corresponding eigenphase sums analysis reported in the two panels of Figure 3.

They show in more detail the behaviour of the two resonances which we found for the A_2 and B_1 transient negative ions (TNIs) of the phenyl molecule computed from the corresponding average of the singlet and triplet cross sections as outlined in the previous discussion.

By fitting with the well-known Breit-Wigner formula [33] each of the associated eigenphase sums in the above symmetry contributions, we extract the pure resonant component from the background thus obtaining the

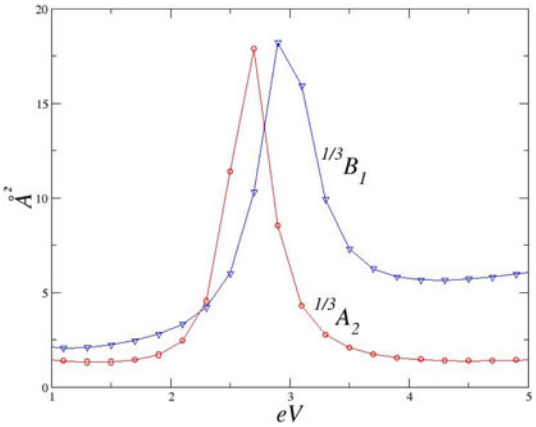

Fig. 2. Computed partial elastic rotationally-summed cross sections in the region of the resonances pertaining to the phenyl molecule.

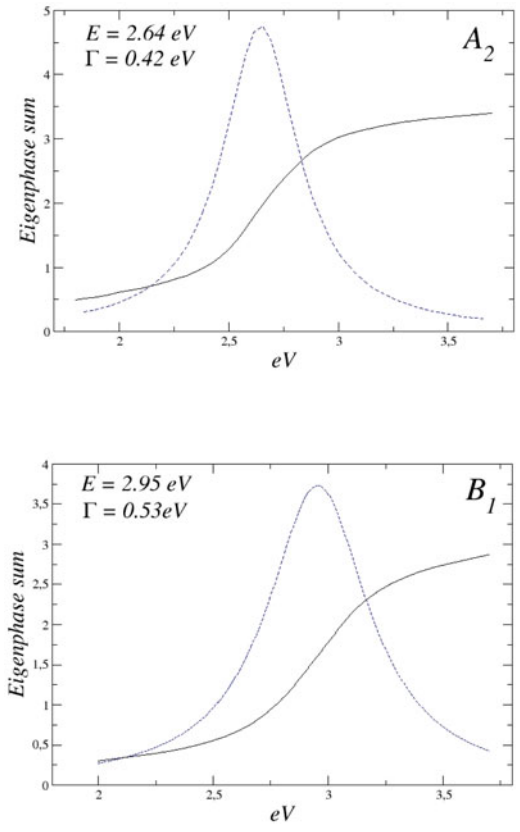

Fig. 3. Detailed analysis of the eigenphase sum behaviour for the two shape resonances of Figure 2. We also report the energy positions and the associated widths as obtained from a Breit-Wigner analysis, the latter shown by the dashed curves. See main text for further details.

resonance width from the Lorentian fit, therefore locating the two resonances that we shall classify, for simplicity, by omitting the spin notation since they originate by empirically mixing the singlet and triplet anionic resonance cross sections. Thus, they are the A_2 and B_1 phenyl metastable anions at $E = 2.64$ eV and 2.95 eV (the eigenphase sum

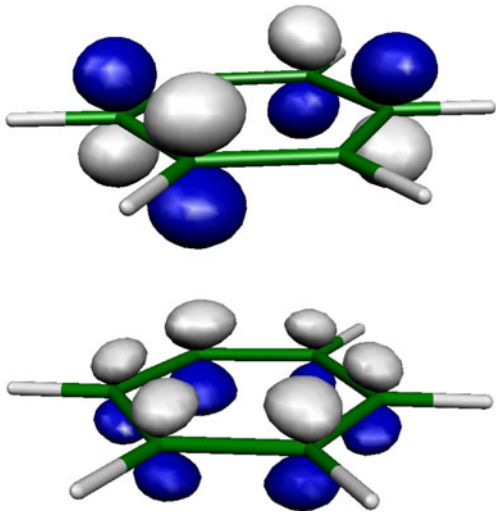

Fig. 4. Upper panel: Spatial shape of the real part of the resonant a_2 wavefunction. Lower panel: The same for the b_1 wavefunction (real part of both of them). Both resonant wavefunctions refer to the phenyl molecule.

having a clear π-jump around each of them) and having a lifetime of 0.16×10^{-14} and 0.12×10^{-14} s, respectively.

It is also interesting at this point to look at the spatial distributions of the scattering wavefunctions (real parts) at the resonant energies in order to link, albeit qualitatively, their distributions over the network of the bound nuclei at the equilibrium geometry with possible coupling effects with the vibrational motion.

In the two panels of Figure 4 we report our computed scattering wavefunctions for the A_2 resonance ($E =$ 2.64 eV, upper panel) and for the B_1 resonance ($E =$ 2.95 eV, lower panel).

The first one shows antisymmetric features with respect to both the symmetry planes of the molecule. The second resonance represents a metastable bound state with clear π^*-like character in which the extra electron is localized well above and below the aromatic ring and is now antisymmetric with respect the molecular plane.

One should also note that the elastic scattering cross sections and, more in detail, the elastic angular distributions (see [26]) can be used as a probe for the interaction potential. However, in order to correctly obtain them within the present Body-Fixed description of the scattering process outlined in the previous Section, the dipolar nature of the target needs to be taken into account. We have done it via the inclusion of the Born correction for the higher partial waves, following the method already described by us in our earlier work [26,31]. Accordingly, we report the final, converged, differential cross sections (DCS) at the energies of the observed resonances in the two panels of Figure 5.

One notices for both resonances the presence of backward scattering in the elastic channels, indicative of an interaction mainly involving short-range potential terms, while the forward scattering, more linked to an interaction due to long-range potential terms, dominates the scattering for both energies. Hence, we could argue that

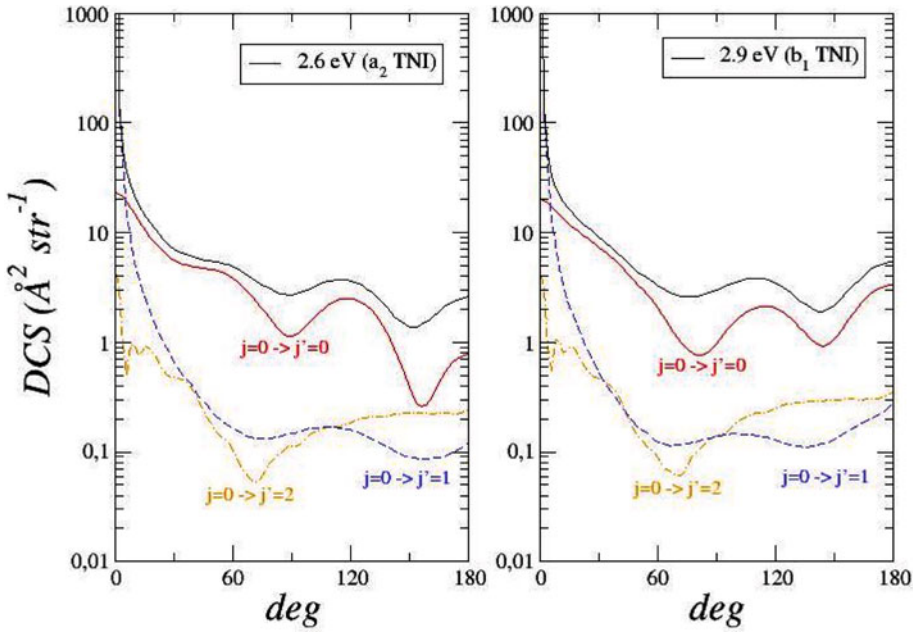

Fig. 5. Differential cross sections (DCS) at the energies of the observed resonances for the phenyl molecule (left: A_2 resonance at 2.6 eV; right: B_1 resonance at 2.9 eV).

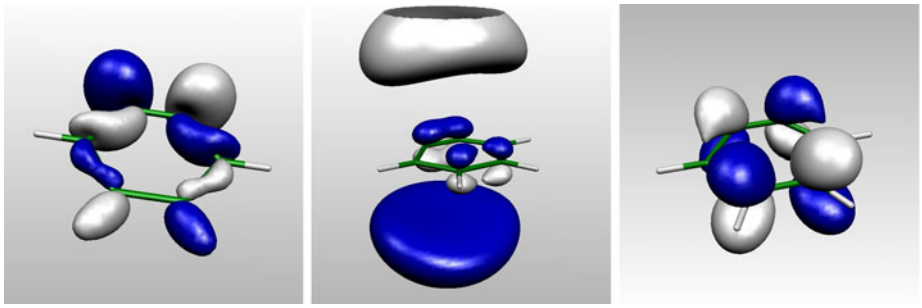

Fig. 6. Computed resonant scattering wavefunctions (real parts) for the three lowest resonances found for the o-benzyne system; from left to right: $^2b_2^*$ at 1.05 eV, $^2b_1^*$ at 2.3 eV and $^2a_2^*$ at 3.3 eV. See text for further details.

the different behaviour of the backward scattering with respect to the forward, small-angle region, indicates that in both cases the dipole scattering (that drives in the forward direction the scattered flux of electrons) is the chief component and, since it corresponds to the $l = 1$ multipole, also matches the $l = 1$, π^*-like features of both resonant electron states. One should also note here that the positions and features of such resonant states are mainly due to the short-range terms of the full interaction employed in our work since the metastable electron is finally located within the same configuration space as that occupied by the lower-lying bound electrons. We find also useful to emphasize that the three-dimensional map for the b_1* resonant wave function of phenyl reveals a metastable bound state in which the extra electron density distribution closely resembles the one found for the 2.286 eV resonance with the same partial symmetry for the ortho-benzyne molecule [16] at its equilibrium geometry. The lower energy needed to temporarily capture the impinging electron in the o-benzyne would also suggest that the stronger permanent dipole of the latter plays a crucial role in decreasing the kinetic barrier responsible for the shape resonance, thereby stabilizing the metastable complex in this channel at a lower collision energy.

The panels of Figure 6 further show, for better clarity, the three maps associated with the TNI states of o-benzyne already discussed by the earlier work of [16]: all 3D shapes of the real parts of the associated wavefunctions are given here for the first time. We shall further discuss these resonant wavefunctions in the following subsection.

On the basis of the shape of the two phenyl's resonant wave functions, we note that our calculations do not show the presence of any σ^* resonance, so that we can surmise that dissociative electron attachment (DEA) channels may not be coming from the above resonant capture processes since the associated electron densities suggest little coupling between the resonant electron and the nuclear bonding network. On the other hand, the additional, possible existence of vibrational Feshbach-type resonances (not present in our model) could very well provide possible paths to stable, de-hydrogenated anions (e.g. $C_6H_4^-$) for the present molecular partner. Hence, what our work

suggests here is that, in both systems, the present paths to anionic stabilization may lead to the formation of main molecular anions, an aspect which we shall further discuss below.

3.3 The anionic quasi-bound states: a structural view

The calculations described in the previous section view the physical process associated with the gas-phase interaction of both phenyl and o-benzyne with low-energy continuum electrons as a dynamical event whereby the specific features of the interaction potential, which describe the response of the electronic structure of the target molecules to the perturbative effects of the impinging electron, are causing the formation of anionic quasi-bound states coupled with the continuum at specific energies of that electron. In other words, when scanning the energy continuum via the scattering electron (chiefly in the low-range of a few eV) we find that transient negative ions (TNIs) are formed into specific symmetry identifiers of the molecular system.

Since the calculations for the scattering cross sections have been presented at the geometry of the neutral molecules (the fixed-nuclei approximation for the collisional event, FNA) it is also of interest to see what could be gleaned about such one-electron excitations of the anionic compounds by carrying out structural, time-independent calculations of the excited bound (more properly, physically quasi-bound) states generated via quantum chemistry. Such calculations do not include the continuum into which the anion's excited states are physically embedded but produce instead a discretization of the continuum space by mapping it via the excited states of the anion computed within the chosen basis set expansion. The calculations have been carried out by employing the method for excited states described in reference [40] and different sizes of the initial basis set expansions have been tested. We have also repeated the calculations with the largest basis set employed by adding the correlation effects included in the DFT calculations, as we shall further discuss below.

Given the physical nature of the problem, we have computed the molecular anions of phenyl and o-benzyne together with their lower-lying excited states, at the nuclear equilibrium geometry of the neutral molecules: as in the scattering calculations, therefore, no nuclear relaxation upon formation of stable anions is included.

Given the crucial role played by correlation forces in stabilizing the anionic state with respect to the neutral, it is not at all straightforward to computationally obtain positive (and small) EA [41]. However, the use of extended basis sets within an Unrestricted Hartree Fock (UHF) approach can be used as a starting point to generate at least partial correlation effects between anionic states while recovering a sort of orbital description of the excited anionic electrons that we shall outline below. The further use of the DFT approach additionally allows us to have a more correlated description for the virtual anionic excitation and therefore more realistic estimates of the EA values. In the present cases, in fact, and considering that we are calculating the vertical EAs for both systems, we find: 0.16 eV and 0.66 eV for phenyl and o-benzyne respectively. These values are definitely smaller than the experimental adiabatic EAs reported earlier, but also indicate the better description of correlation within the bound electrons afforded by the DFT approach. In the present study, after testing several choices of possible basis sets, we have finally employed the aug-cc-pv5z basis set expansion [40], either within the configuration interaction (CI) approach or directly within DFT calculations for both neutrals and anions. The present CI(S) approach with an extended basis set has been finally selected to allow us to generate for both systems a fairly dense discretization of the anionic continua, in order to be able to match and reproduce the metastable resonant features obtained from the scattering calculations, although no explicit calculations of actual excitation energies have been employed.

The following comments could be made by perusing our CI(S) calculations:

(i) both systems, at the level of correlation warranted by a CI(S) within our extended basis set expansion, provide bound anion at the geometry of each of the neutrals: of $^1A_1$ symmetry for phenyl and of $^2B_2$ for o-benzyne. They yield, however, small and negative EA values;

(ii) the anionic excitation energies into the continuum cover an energy range between ∼2 and ∼4 eV to help us to qualitatively match the scattering resonances seen in both systems in the previous section. Since the highest, excited states are less accurate than the lower ones, we limited our comparison to finding a correspondence between the lower excited states of that symmetry and our scattering resonances for each molecule.

(iii) It is also interesting to note that the two sets of calculations have different energy reference levels: it is the neutral target for the scattering calculations but is instead the anionic target for the structural calculations. Since the physical difference between such reference states is their vertical EA values, we have empirically shifted the positions of the quasi-bound states close to our resonant states by 0.66 eV and 0.16 eV, respectively, for the phenyl and the o-benzyne systems, those being the EA values obtained from our DFT calculations, as discussed earlier.

The data in Table 1 compare the shifted energies of the quasi-bound states with the lowest scattering TNI found for the same symmetries.

When looking at the comparison for the phenyl anion we see that both the TNIs located by our scattering calculations are present within the CI formulation of the excitation processes. One should also note at this point that the scattering calculations, as already mentioned in the previous sections, are carried out by generating 'hybrid' singlet and triplet cross sections for the anionic species originating from a neutral phenyl radical. This means that the scattering orbitals are a mixture of a singlet and triplet states while the structural calculations,

Table 1. Energy-shifted (quasi-bound) excited anionic states of phenyl and o-benzyne in comparison with the lowest resonances (TNIs) obtained via scattering calculations (all energies are in eV).

	CI(S) calcs.	Scattering calcs.
Phenyl		
$^1A_2^* \leftarrow {}^1A_1$	2.92	2.64
$^3A_2^* \leftarrow {}^1A_1$	2.64	
$^1B_1^* \leftarrow {}^1A_1$	2.64/3.13	2.95
$^3B_1^* \leftarrow {}^1A_1$	2.58/3.13	
o-Benzyne		
$^2B_2^* \leftarrow {}^2B_2$	1.66	1.05
$^2B_1^* \leftarrow {}^2B_2$	2.24/2.76	2.30
$^2A_2^* \leftarrow {}^2B_2$	3.11	3.30

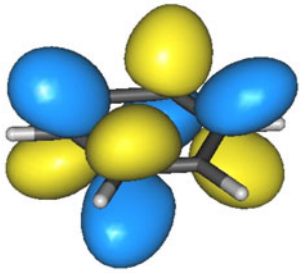

Fig. 7. Computed 3D maps of the excited anionic state a_2^* of the phenyl molecule from the CI quantum calculations. See text for further details.

on the other hand, were separately carried out for singlet and triplet states. Hence, the energy differences found in Table 1 could therefore be explained by the averaging between states performed by the scattering calculations. The lowest scattering resonance is associated with the $^1A_2^*$ and $^3A_2^*$ excited states which are now at 2.92 and 2.64 eV, i.e. fairly close to the scattering value. Furthermore, Figure 7 shows the 3D spatial map of the extra electron for the singlet excitation from the CI procedure. In each specific electronic excited state of the pseudo-bound anion, the localization of the extra electron has been estimated by a linear combination of the highest occupied molecular orbitals of each determinants of the CI(S). The mixing coefficients are taken from the CI(S) expansion: it is therefore a sort of a CI view of the added electron in that excited anionic state. The figure shows that indeed the spatial distribution and its nodal structure are of the same shape and structure as that shown by the scattering electron reported in the upper panel of Figure 4. Thus, it is reasonable to suggest that the lowest $^1A_2$ and $^3A_2$ excited states produced by the CI(S) calculations correspond to a scattering state of the same symmetry obtained directly from dynamical calculations.

When we now examine the next resonant state found for the phenyl molecule in the low-energy region, we see in Table 1 that two, fairly close excited states of the same molecule are produced by the CI(S) calculations for the singlet and triplet states around 2.90 eV, i.e. near the

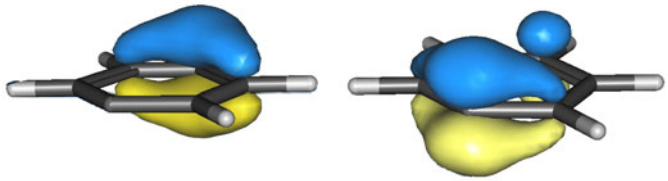

Fig. 8. Computed 3D maps of two different excited quasi-bound electrons for the phenyl anion of B_1^* symmetry produced by the CI(S) structure calculations. See text for further details.

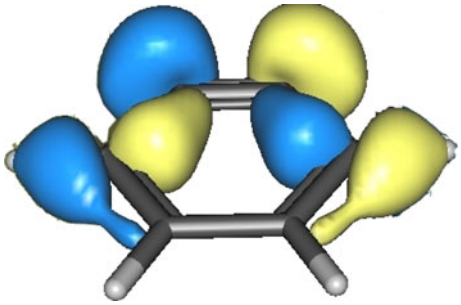

Fig. 9. Computed 3D map of the electronically excited anion of o-benzyne of b_2^* symmetry from the CI(S) calculations. See main text for further details.

energy position of the scattering calculations for the resonance, which we found around 2.95 eV. The corresponding 3D maps associated with the virtual electrons belonging to two different singlet quasi-bound states, generated with the same procedure already described for Figure 7, are given by Figure 8 and clearly indicate that, as expected, the limited correlation between bound and virtual electrons afforded by the present CI(S) treatment is producing excited electrons that do not compactly describe the resonance. In fact we see that two, very close, different excited states of the anion are needed to describe the highly correlated, π^*-like nature of the resonant scattering state in this symmetry. A qualitative combination of the two 3D views of Figure 8, on the other hand, turns out to reproduce quite closely the spatial distribution of the scattering electron of the same symmetry given by Figure 4.

If we now turn to the case of o-benzyne, the data given by Table 1 indicate again that the first excited anionic state from the CI(S) calculations, using the very extended basis set discussed earlier, is a $^2B_2^*$ state located into the continuum of the ground state anion (also of $^2B_2^*$ symmetry) at 1.36 eV. The corresponding TNI obtained from the scattering calculations is also a $^2B_2^*$ anion and is located at 1.05 eV. Furthermore, the 3D map of the CI-like wave function for the extra-electron from the SOMO calculations (Fig. 9) provides the same 3D view as that given by Figure 6 from the scattering calculations at the same symmetry.

It therefore seems convincing, given the agreement between these two very different approaches, that o-benzyne presents a resonant, metastable anionic state of $^2B_2^*$ symmetry at positive energies around 1 eV of collision energy.

In other words, we can reasonably surmise that using the spatial distributions of the relevant MOs as a tool for

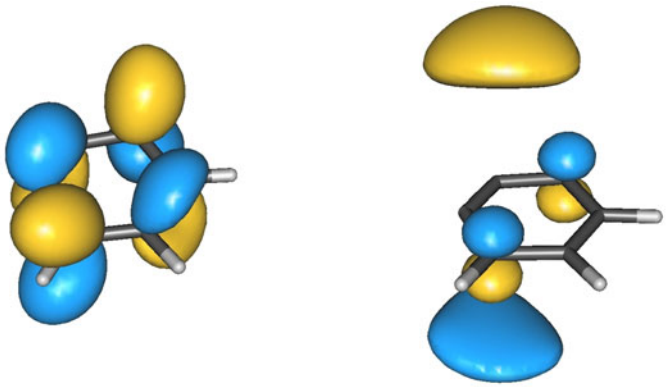

Fig. 10. Computed spatial maps of the two different excited states of the o-benzyne of b_1^* symmetry from the CI(S) calculations.

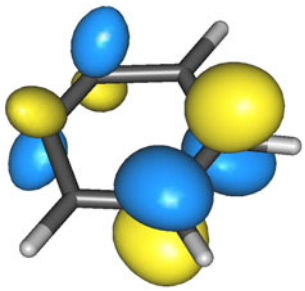

Fig. 11. Computed spatial distribution of the a_2^* CI-Like wave function for the SOMO associated with quasi-bound, excited state of the o-benzyne anion. See main text for further details.

comparison helps us to select which region of the continuum anionic subspace, artificially discretized by the CI calculations, is more likely to represent the resonances found by the physically more correct scattering calculations. If one further considers the natural width associated with the scattering resonances (e.g. 0.61 eV for the present b_2^* resonant state), we can conclude that the present comparison between structural and scattering calculations is yielding fairly realistic results for such anion.

We now turn to a comparison between the CI(S) excitations provided by structural calculations and the next two higher scattering resonances present for the o-benzyne target, so that we could check if such higher excited states from a partially correlated anionic calculation would be able to find the higher TNIs surmised by the scattering calculations and given, for o-benzyne, by the 3D maps of Figure 6, central and right panels respectively. The calculations reported by Table 1 now indicate that the resonance around 2.30 eV, which presents again a strong, highly correlated π^*-like character, can be associated to two different, but close in energy, excited states of the anion with the same symmetry: at 2.24 and 2.76 eV respectively. The corresponding spatial CI-like maps of the two extra electrons associated with the CI(S) calculations are given by Figure 10. We see here, once more, the same correlation problem already discussed for the phenyl molecule before: the π^*-like nature of the scattering resonance requires an higher level of correlation than the one introduced by our structure calculations, and therefore we see in the latter the presence of two virtual orbitals needed to describe the scattered electron at the resonance.

The results for the third resonance for o-benzyne indicate it to be around 3.30 eV: the data in Table 1 show a virtual state of the same symmetry, produced by the CI(S) calculations at 3.11 eV. The corresponding 3D, CI-like map of the extra excited electron is given by Figure 11, where we clearly see that the spatial features for it are very similar to those reported in the right panel of Figure 6. We can therefore conclude that, at least qualitatively, all the low-energy shape resonances found for the two title systems are also well accounted for by the CI(S) structural calculations. The latter results, in fact, find the same resonances at energies close to those from the scattering results and also find them to be very similar in spatial shapes.

3.4 The near-threshold scattering wavefunction

In the present section we shall provide a more detailed analysis of the behaviour of both phenyl and benzyne polar targets under very-low energy electron collisions, focusing on the shapes of the continuum electron wave functions. Our computed scattering electron wave function for the e-C_6H_5 is shown in Figure 12, where, from top to bottom, we report it at 10^{-1}, 10^{-2} and 10^{-3} eV, respectively. The same set of results are shown for the benzyne molecule by Figure 13.

Generally speaking, there has been great interest in electron interactions with polar targets both in the positive- and the negative-energy regimes, since the presence of the permanent electric dipole of the target can affect both scattering wavefunctions and weakly bound, Rydberg-like anionic states [34,35].

As each panel of both Figures 12 and 13 clearly shows, the scattering wave function for the extra-electron has a node located on the plane on which the molecule itself rests: it separates the so-called valence part (positive phase, represented in grey) and the extended part (negative phase, in blue). The great majority of the continuum electron is located outside the molecular frame and on the positive side of the permanent dipole. Going down in collision energy, i.e. moving from top to bottom in the figures, the above nodal plane remains present while the general behaviour of the wavefunctions is to further move away from the molecular nuclear structure. Could one justify, at least qualitatively, such a behaviour in the framework of the scattering of slow electrons by polar molecules?

To provide an answer, it is worth to keep in mind that most past theoretical analysis of electron-dipole scattering have looked at a point-dipole model [36,37], for which the main disadvantage consists in modifying at the origin the r^{-2} singularity so that simpler formulae for the wave function cannot be directly used. The well known 'physical dipole' model (also fixed finite dipole, FFD), where an equal magnitude positive and negative point charges are

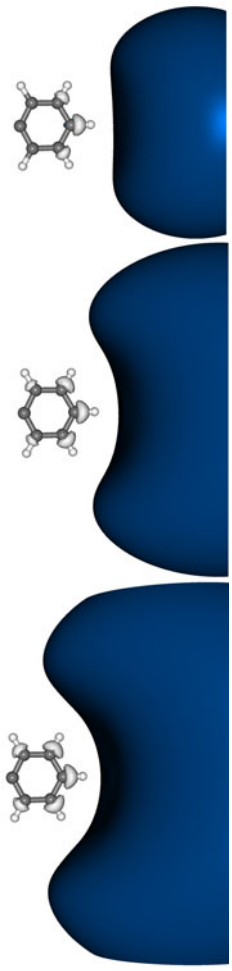

Fig. 12. From top to bottom: Scattering wave function at 10^{-1}, 10^{-2} and 10^{-3} eV for the phenyl molecule. See main text for details.

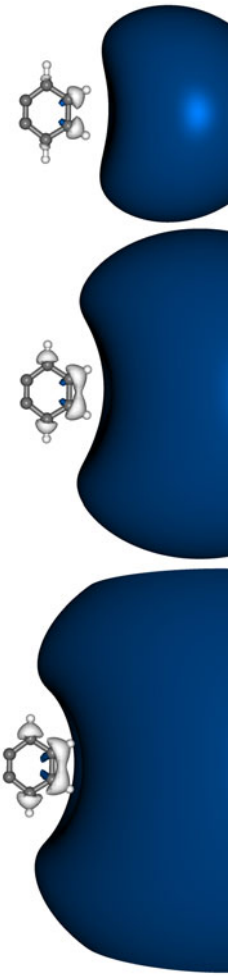

Fig. 13. Same calculations as those of Figure 12 but this time involving the o-benzyne. See main text for details.

separated by a finite distance d is undoubtly a theoretical improvement, since in the latter case the potential has no difficulties at the origin or at each of the charges [35]. Both models, however, were shown to yield the same critical dipole moment value [38], $\mu_c = 1.625$ D (equivalently 1.625×10^{-18} esu cm or 0.639 a.u.), which, in the framework of an electron moving in a 'bare' fixed dipole potential, is the needed value to bind it in a σ bound state. Moreover, we know that the primary deficiencies of the simple PD and FFD models are the absence of both Coulomb (repulsive) and exchange (attractive) potential terms produced by the neutral target electrons, as well as the absence of orthogonality of the extra-electron's orbital to those of the valence bound electrons, a feature also enforced in our scattering calculations. Such features have been already discussed for the e-H_2S molecule, the latter having a permanent dipole of 0.99 D [39] which is not far from that of the present molecule, $\mu_{\text{phenyl}} = 0.872$ D.

In this framework, therefore, our model indeed accounts for the electron-dipole interaction with an ab-initio approach which resembles the PD model and goes beyond it, since we also account for the whole electronic distribution on the target molecule. Furthermore, the present calculations make use of the orthogonality condition between the scattered electronic wave function and the N-electron wave function of the neutral target, which in fact produces the requested nodal plane typical of a dipole state.

Since the permanent dipole provides a long-range force which is also important in the short-range for low-energy collisions (when low-order partial-wave scattering is considered), then one should keep in mind that inelastic energy transfers can further play an important role here since the impinging electron might be also temporarily held near the target molecule by rotational excitation of the latter. Hence, the threshold-energy colliding electron could loose enough energy in forming a quasi-bound (metastable) zero-energy virtual state in the field of the dipole. Its ensuing autodetachment would supply electrons back into the low-density gaseous medium, thus providing an additional contribution to the momentum-transfer cross section. This effect could have important repercussions on the mean drift velocity of low-energy electrons

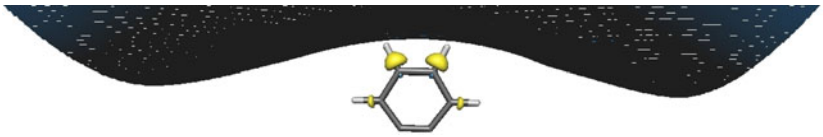

Fig. 14. Computed SOMO orbital for the o-benzyne anion at the UHF level of calculations. See main text for further details.

crossing an interstellar region where both the phenyl and the o-benzyne are likely to be present.

The same description of near-threshold scattering wavefunction for o-benzyne is reported by Figure 14, where we clearly see similarities with the findings discussed above for the phenyl molecule. The data for both polar systems clearly show, at collision energies in the meV range, the presence of scattering states located outside the molecule on the positive side of the permanent molecular dipole and therefore away from the reactive triple bond region. Since, in the case of o-benzyne, the experimental dipole moment is close in size to the critical value (1.67 D), its value should cause the formation of an infinity of bound states and, in particular, the occurrence of bound anionic states with very small EA, describing an excited dipolar anion with a very diffuse bound electron: the dipole-bound state (DBS). The latter, weakly bound electron could be spatially distributed within the same region of the dipole orientation [42,43] as found for the present scattering states.

To this end, we have therefore carried out additional structure calculations for the o-benzyne anion, at the geometry of the neutral molecule, to see if one can find asymptotically bound electrons to the neutral, since the additional, Rydberg-like electron is expected to cause very little distortion of the valence electron density of the neutral partner.

We have carried out calculations at the aug-cc-pv5z level of expansion described in the previous sections and also added an extended series of diffuse gaussians as discussed for similar calculations for HOCO [44] and several anionic polyynes [45].

The calculations have indeed provided a DBS state of the o-benzyne anion, and the map of the corresponding SOMO is reported by Figure 14.

The calculations of the anionic state of Figure 14 were carried out at the UHF level so that, albeit using a very extended basis set, no correlation were included in the variational study. This means that, given the rather weak binding strength of the anionic state of o-benzyne, we obtain a very diffuse anion for which the Koopman theorem yields here a positive eigenvalue of ∼0.13 eV, thus suggesting that this anionic state is describing a Rydberg-like anion very similar in structure to a dipole bound state (DBS) of o-benzyne, although the still missing portion of dynamical correlation not sufficiently described by the CI(S) calculations does not manage to obtain a negative, albeit very small, eigenvalue for such an extra bound state.

When one is further introducing additional correlation contributions, here at the level of DFT calculations, one drops down in energy to the description of the more strongly bound valence anionic state of the correct $^2B_2$ symmetry: its spatial shape is now reported by the SOMO wavefunction of Figure 15.

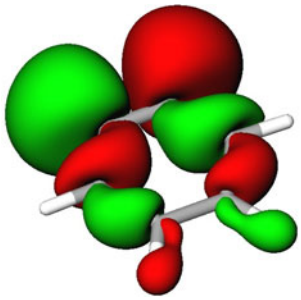

Fig. 15. Computed SOMO orbital for the valence anionic state ($^2B_2$) of the o-benzyne molecule. See main text for further details.

One clearly sees there that the inclusion of additional correlation effects allows now the quantum structure calculations to produce the ground state anionic configuration which corresponds the valence anionic state, in which the extra electron is strongly localized onto the molecular structure of the target and is very different from the diffuse, Rydberg-like anionic state reported by Figure 14 and obtained as described before for the weakly bound DBS state.

Thus, we have seen above that the o-benzyne molecule, given the near-critical value of its permanent dipole moment, is indeed capable of having, at very low collision energies, scattering states of its excited anions into the continuum which are driven by its charge-dipole interaction as discussed before and that could be termed as dipole scattering states (DSSs) close to threshold. Additionally, the quantum structure calculations on the same molecule have shown that correlation forces between bound electrons are essential for producing a bound anion (at the geometry of the neutral) where the extra electron occupies a valence, bound SOMO of the system (see Fig. 15). We have also shown that, for the same molecular target, the HF calculations with very large, diffuse basis set expansions are able to support an anionic state which is only very weakly bound and which strongly resembles a DBS state of the anion: its spatial representation in Figure 14 is indeed very similar to the DSS states of Figure 13 for the same molecule and therefore we could argue that one likely path to initial stabilization of a bound anion of o-benzyne could either be by radiative stabilization (RS) of one of its DSS states into the corresponding DBS state, or by collisional energy redistribution of the small amount of available excess energy, followed by the initial binding of the extra electron into a DBS state. The latter is now a weakly bound state which can further decay down

into the valence, bound anion by additional, larger energy redistribution processes within the 'largely collisionless' environment of the ISM scenarios we are considering.

4 Present conclusions

In this paper we have analysed in some detail the possible presence of metastable anions, formed by low-energy electron attachment to the neutral species, for two polar aromatic molecules which are considered as precursor species in condensation reactions leading to the formation of larger aromatic molecules occurring in the structures of polycyclic aromatic hydrocarbons.

In particular we have analysed metastable and bound anions for the phenyl (C_6H_5) molecule, a very reactive radical, and for the o-benzyne molecule, also a very reactive partner through the role known to be played by its triple bond.

We have carried out two different types of calculations to give more confidence to the results obtained in this work: (i) quantum scattering calculations via multichannel expansion to locate the low-energy shape resonances in phenyl; and (ii) quantum structure calculations for the ground state anions of both phenyl and o-benzyne using extended basis set at the UHF level, followed by configuration interaction calculations for single excitations into the orbitals of excited anions at the geometries of the neutral species. The second set of calculations allowed us to additionally obtain an approximate discretization of the anionic continuum in order to compare the excited anionic configurations, obtained with that method, and the corresponding metastable anions more correctly given by the scattering calculations of the first set of data.

The use of 3D, CI-like maps for the active, excited electrons in such quasi-bound anionic states has allowed us to carry out a qualitative match between the scattering resonant wavefunctions, at specific positive energy, and the excited MOs produced by the CI(S) procedure in the structure calculations.

We have further explored the ultra-low energies of the scattered electron by looking at the behaviour of the continuum wavefunction, for both phenyl and o-benzyne, at collision energies down to a few meV, where the inelastic couplings between the scattering electron and the molecular internal rotational levels is known to be more efficient [16]. We have found that the scattering behaviour at such energies is largely controlled by the dipolar interaction and therefore the scattered electron wavefunction is dominated by $\ell = 0, 1$ waves and remains on the outskirts of the molecular charge distribution of the neutral partners, as shown by Figures 12 and 13.

The presence of a near-critical dipole value for o-benzyne further suggests the possible existence of dipole bound states (DBS) in this molecule, i.e. of a weakly bound negative ion with a very small EA. One of such states is in fact located by us for o-benzyne, as discussed in the previous section, and therefore one can suggest possible paths for the final formation of o-benzyne stable anions: either radiative or collisionally inelastic stabilization of dipole scattering states at ultralow collision energies into the corresponding dipole bound states, which can eventually decay into valence bound anionic states (for this molecule, at further 500 meV down in energy), given the essentially collisionless environments discussed here for the title molecules.

Although such states do not exist for the phenyl molecule, our present calculations suggest that its permanent dipole is strong enough to obtain DSS states of the scattered electron near threshold, in the meV energy range. The latter could therefore be also involved, together with the two higher shape resonances into stabilization paths toward the production of ground state, bound valence anions of these polar molecules.

The financial supports of the PRIN 2009 National Research Project and of the COST-Action CM805 "The Chemical Cosmos" are gratefully acknowledged. The computational support via an ISCRA grant from the CINECA Consortium is also gratefully acknowledged. We are also grateful to all the referees for all their valuable suggestions for improving the presentation of our work.

Note added in proof. After the work described in the present paper had reached the proofs stage, we were made aware of a recent publication (10 September 2013) which has appeared in the *Journal of Chemical Physics* (139, 104308) in which the author presents model calculations for the o-benzyne low-energy electron scattering and claims that the $^2B_2$ temporary anion is instead a proper, bound negative ion of that system. The calculations of the present paper, which use both scattering calculations and CI calculations with large basis sets, show instead very cleary that the o-benzyne anion has a $^2B_2$ bound state but also a $^2B_2$ resonant state orthogonal to the latter, not in agreement with the conclusions of the above-mentioned publication.

References

1. A.G.G.M. Tielens, in *The Physics and Chemistry of the Interstellar Medium* (Cambridge University Press, Cambridge, 2005)
2. A.G.G.M. Tielens, in *PAHs and the Universe* (EAS Publications, 2011), Vol. 46, p. 3
3. F. Salama et al., ApJ **728**, 154 (2011)
4. C.W. Bauschlicher et al., ApJS **189**, 341 (2010)
5. T.P. Snow, V.M. Bierbaum, Annu. Rev. Anal. Chem. **1**, 229 (2008)
6. J.P. Maier et al., ApJ **726**, 41 (2011)
7. T. Oka, B.J. McCall, Science **331**, 293 (2011)
8. J. Cernicharo et al., ApJ **546**, L123 (2001)
9. P. Ehrenfreund, A.M. Sephton, Faraday Discuss. **133**, 277 (2006)
10. A.G.G.M. Tielens, *Proc. Int. Astr. Union*, edited by J. Cernicharo, R. Bachiller (Cambridge University Press, Cambridge, 2011), Vol. 280
11. S. Kwok, in *The Origin and Evolution of Planetary Nebulae* (Cambridge University Press, Cambridge, 2000)

12. S. Kwok, ApJ **198**, 583 (1975)
13. J.H. Black, *Proc. Int. Astr. Union*, edited by J. Cernicharo, R. Bachiller (Cambridge University Press, 2011), Vol. 280
14. D.M. Hudgins, L.J. Allamandola, ApJ **516**, L41 (1999)
15. S. Kwok, K. Volk, P. Bernath, ApJ **554**, L87 (2001)
16. F. Carelli, F. Sebastianelli, I. Baccarelli, F.A. Gianturco, ApJ **712**, 445 (2010)
17. F. Carelli, F. Sebastianelli, M. Satta, F.A. Gianturco, MNRAS **415**, 425 (2011)
18. R.F. Gunion, M.K. Gilles, M.L. Polak, W.C. Lineberger, Int. J. Mass Spectrom. Ion Proc. **117**, 601 (1992)
19. P.G. Wenthold, R.R. Squires, W.C. Lineberger, J. Am. Chem. Soc. **120**, 5279 (1998)
20. R.J. McMahon et al., ApJ **590**, L61 (2003)
21. E. Kraka, D. Cremer, Chem. Phys. Lett. **216**, 333 (1993)
22. S. Lepp, A. Dalgarno, ApJ **324**, 553 (1988)
23. V. Wakelam, E. Herbst, ApJ **680**, 371 (2008)
24. N.J. Demarais, Z. Yang, O. Martinez Jr., N. Wehres, T.P. Snow, V.M. Bierbaum, ApJ **746**, 32 (2012)
25. R.R. Lucchese, F.A. Gianturco, Int. Rev. Phys. Chem. **15**, 429 (1996)
26. F.A. Gianturco, P. Paioletti, in *Novel Aspect of Electron-Molecule Collisions*, edited by K.H. Becker (World Scientific, 1998)
27. N. Sanna, F.A. Gianturco, in *Photon and Electron Collisions with Atoms and Molecules*, edited by P.G. Burke, C.J. Joachain (Plenum, New York, 1997)
28. S.L. Altman, A.P. Cracknell, Rev. Mod. Phys. **37**, 19 (1965)
29. S. Hara, J. Phys. Soc. Jpn **22**, 710 (1967)
30. R. Curik, F.A. Gianturco, R.R. Lucchese, N. Sanna, J. Phys. B **34**, 59 (2001)
31. F.A. Gianturco, A. Jain, Phys. Rep. **143**, 348 (1986)
32. M.J. Frisch et al., *Gaussian 03* (Gaussian, Inc., Wallingford CT, 2004)
33. R.J. Taylor, *Scattering Theory* (John Wiley & Sons, New York, 1972)
34. J. Simons, J. Phys. Chem. A **112**, 6401 (2008)
35. G.A. Gallup, Phys. Rev. A **80**, 012511 (2009)
36. O.H. Crawford, Proc. Roy. Soc. (London) **91**, 279 (1967)
37. A. Dalgarno, Chem. Phys. Lett. **1**, 23 (1967)
38. J.E. Turner, Am. J. Phys. **45**, 758 (1977)
39. NIST, Computational Chemistry Comparison and Benchmark Database
40. J.B. Foresman, M. Head-Gordon, J.A. Pople, M.J. Frisch, Phys. Chem. **96**, 135 (1992)
41. P.G. Wenthold, J. Hu, R.R. Squires, J. Am. Chem. Soc. **118**, 11865 (1996)
42. S. Cales, C. Desfrançois, J.P. Schermann, D.M.A. Smith, L. Adamovicz, J. Chem. Phys. **112**, 3726 (2000)
43. J. Simons, Acc. Chem. Res. **39**, 772 (2006)
44. S. Miyabe, D.J. Haxton, K.V. Lawler, A.E. Orel, C.W. McCurdy, T.N. Rescigno, Phys. Rev. A **83**, 043401 (2011)
45. F. Carelli, T. Grassi, M. Satta, F.A. Gianturco, ApJ **774**, 97 (2013)